Structure properties relationship study of electron-deficient dihydroindeno [2,1-b]fluorene derivatives for n-type Organic Field Effect Transistors.

Maxime Romain, Michèle Chevrier, Sarah Bebiche, Tayeb Mohammed-Brahim, Joëlle Rault-Berthelot, Emmanuel Jacques, Cyril Poriel

Structure properties relationship study of electron-deficient dihydroindeno [2,1-*b*]fluorene derivatives for n-type Organic Field Effect Transistors[*]

Maxime Romain,[a] Michèle Chevrier,[a] Sarah Bebiche,[b] Tayeb Mohammed-Brahim,[b] Joëlle Rault-Berthelot,[a] Emmanuel Jacques[b*] Cyril Poriel[a*]

[a] *UMR CNRS 6226-Institut des Sciences Chimiques de Rennes- Équipe Matière Condensée et Systèmes Électroactifs, Bat 10C, Campus de Beaulieu - 35042 Rennes Cedex France*
[b] *UMR CNRS 6164-Institut d'Électronique et des Télécommunications de Rennes- Département Microélectronique & Microcapteurs, Bât.11B, Université Rennes 1, Campus de Beaulieu 35042 Rennes Cedex, France*

Abstract
A bridged *syn* triphenylene derivative, namely 5,7-dihydroindeno[2,1-*b*]fluorene, functionalized with dicyanovinylene units **(2,1-*b*)-IF(=C(CN)$_2$)$_2$** has been designed, synthesized and characterized. The optical and electrochemical properties have been carefully studied through a combined experimental and theoretical approach and compared to those of three others structurally related dihydro[2,1-*b*]indenofluorene derivatives bearing methylenes, **(2,1-*b*)-IF**, carbonyls, **(2,1-*b*)-IF(=O)$_2$**, or both carbonyl and dicyanovinylene, **(2,1-*b*)-IF(=O)(=C(CN)$_2$)** on the bridgeheads. **(2,1-*b*)-IF(=C(CN)$_2$)$_2$** which possesses a very low LUMO level, ca -3.81 eV, has been successfully used as active layer in n-channel OFETs using epoxy based photoresist SU-8 as gate insulator. **(2,1-*b*)-IF(=C(CN)$_2$)$_2$** based n-channel OFETs show promising properties such as a low threshold voltage functioning of 7.2 V (low gate-source and drain-source voltages), high ratio between the on and the off currents (6.3×10^5), interesting subthreshold swing (SS=2.16) and electron mobility ($>10^{-3}$ cm^2/V.s) and excellent stability under electrical stress. This electrical stability has allowed to incorporate **(2,1-*b*)-IF(=C(CN)$_2$)$_2$** based n-channel OFETs in an integrated circuit. Thus, as a proof of concept, pseudo CMOS inverters made of n-type **(2,1-*b*)-IF(=C(CN)$_2$)$_2$**-based OFETs have been fabricated and characterized highlighting the potential of this new family of materials.

[*] Electronic Supplementary Information (ESI) available:materials and methods, experimental details; synthesis and characterization of all compounds, copy of NMR spectra…

Table of Contents

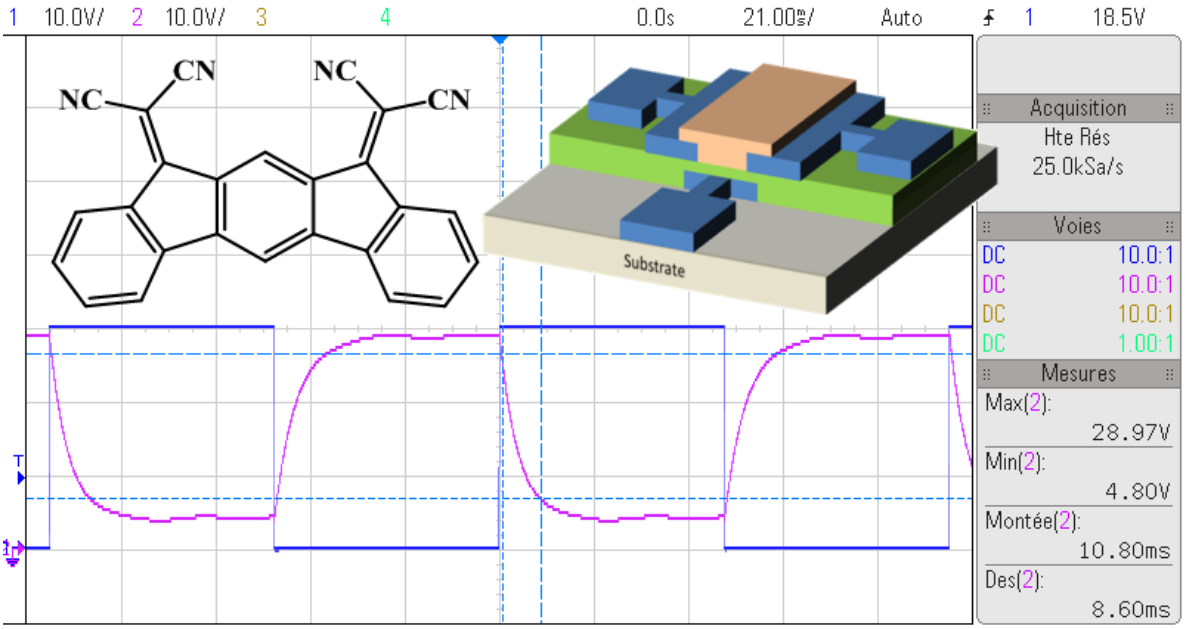

Introduction

Of particular interest in Organic Electronic technology are the electron transporting Organic Field Effect Transistors (n-type OFETs).[1-4] Although the recent impressive progresses have led to electron transporting materials with mobility of negative charges up to unity, the number of n-type molecules is still very limited compared to hole transporting (p-type) molecules.[1-4] Designing new highly efficient semi-conductors for n-type OFETs is hence of particular interest for the future of this technology. In addition, a key point in OFET technology is to obtain integrated organic circuits,[5] which require important OFETs characteristics such as : a low threshold voltage (to decrease supply voltage in circuit), a high on/off current ratio (good discrimination between the on and off state for an efficient switch), good field effect mobility of charge carrier and subthreshold swing (capability to switch between on and off state). However, one of the main problems to achieve an integrated organic circuit is the electrical instability of such devices. This electrical instability has been previously investigated in silicon-based devices and although some debates still exist on the origin of this instability, the main mechanisms have been rationalized.[6] However, in organic electronics, the mechanisms responsible of electrical instability still remain to be elucidated.

Thus, these key parameters for obtaining efficient and stable n-type OFETs for integrated circuits, are directly linked to the properties of the organic semiconductor used as active layer and hence to its molecular design. From a chemical point of view, the design strategy of n-type organic semiconductors usually consists of judicious introduction of electron- withdrawing groups or atoms (carbonyls, dicyanovinylenes, imides, halogens, etc.) to a π-conjugated core to depress the LUMO level without pertubating the intermolecular electron hopping. In addition, the molecular structure should be highly thermally and electrically stable in a device to allow the fabrication of a circuit. The restricted diversity of π-conjugated cores developed to date in literature (mainly based on thiophene or fused thiophene, perylene, naphthalene, phtalocyanine, etc.)[3,7] has led us to focus on other molecular fragments barely investigated, ie. linear bridged extended oligophenylenes. Thus, of particular interest in the oligophenylenes family is the bridged-*para*-terphenyl unit with an *anti* geometry, namely, 6,12-dihydroindeno[1,2-*b*]fluorene, which is nowadays an important building unit for blue OLED applications.[8-15] The potential of the dihydroindeno[1,2-*b*]fluorenyl fragment as a n-type semiconductor in OFET has been also stressed in the literature.[2,16-20] However, the dihydroindeno[1,2-*b*]fluorene is not the only member of the bridged-terphenyl family since it possesses four other positional isomers, which have only started to be investigated very recently (see structures of the 5 isomers in ESI).[11,12,21-31] For example, due to its high triplet state energy level, the 7,12-dihydroindeno[1,2-*a*]fluorene isomer (*Anti* bridged *meta*-terphenyl) has emerged as an interesting host material for blue phosphorescent OLEDs.[31] However, the *meta syn* terphenyl isomer, namely 5,7-dihydroindeno[2,1-*b*]fluorene,[29,30] only recently incorporated in non-doped blue OLEDs with promising performance has been poorly investigated to date and, to the best of our knowledge, has never been designed for n-OFET applications. With this in mind, we report herein a new 5,7-dihydroindeno[2,1-*b*]fluorene derivative, **(2,1-*b*)-IF(=C(CN)$_2$)$_2$**, bearing on the bridgeheads highly electron-deficient dicyanovinylene functionalities. The properties have been studied and compared to those of structurally related dihydroindeno[2,1-*b*]fluorenes bearing on the bridgeheads: methylenes in **(2,1-*b*)-IF**, carbonyls in **(2,1-*b*)-IF(=O)$_2$** and both carbonyl and dicyanovinylene in **(2,1-*b*)-IF(=O)(=C(CN)$_2$)**, (Scheme 1). Finally, **(2,1-*b*)-IF(=C(CN)$_2$)$_2$** has been used as active layer in n-channel OFETs with promising performance and excellent electrical stability under gate bias stress, which have allowed their incorporation in an integrated circuit. As the future of organic electronics is to prepare integrated organic circuits, pseudo CMOS inverters made of n-type **(2,1-*b*)-IF(=C(CN)$_2$)$_2$**-based OFETs have been also fabricated and characterized.

This work is, to the best of our knowledge, the first report on the application of a dihydroindeno[2,1-*b*]fluorene based semiconductor in n-type OFET and highlights the potential of such family of materials to provide integrated organic circuits.

Results and discussion:

Design and Synthesis

The molecular design of the present semi-conductors consists to rigidify the *meta* terphenyl unit by two bridges in a *syn* configuration (Scheme 1). This rigidification by the bridges would increase the flatness (and hence the π-electron delocalization) of the molecular system in order to allow an efficient intermolecular π–π stacking in the solid state, essential for electron hopping. Electron-withdrawing ketones and/or dicyanovinylene functionnalities have been introduced on the bridgeheads of the dihydroindeno[2,1-*b*]fluorenyl core strongly depressing the LUMO energy level without disrupting the π-conjugation, which is crucial for achieving efficient electron injection/transport.

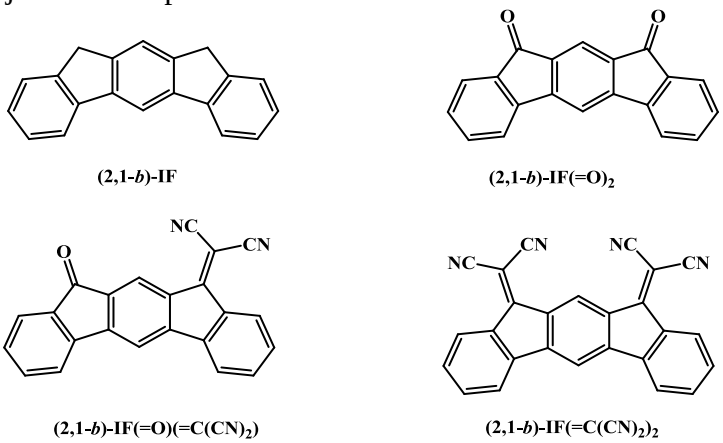

(2,1-*b*)-IF **(2,1-*b*)-IF(=O)$_2$** **(2,1-*b*)-IF(=O)(=C(CN)$_2$)** **(2,1-*b*)-IF(=C(CN)$_2$)$_2$**

Scheme 1 The four 5,7-dihydroindeno[2,1-*b*]fluorene derivatives investigated in this work: **(2,1-*b*)-IF**, **(2,1-*b*)-IF(=O)$_2$**, **(2,1-*b*)-IF(=O)(=C(CN)$_2$)** and **(2,1-*b*)-IF(=C(CN)$_2$)$_2$.**

The synthesis of **(2,1-*b*)-IF(=C(CN)$_2$)$_2$** involved the synthesis of the key fragment **(2,1-*b*)-IF(=O)$_2$** (see ESI for synthetic details). Thus, the synthesis of (**2,1-*b*)-IF(=O)$_2$** has been envisaged through an efficient approach (Scheme 2) based on the intramolecular electrophilic bicyclization of terphenyl **4** with the ester groups on the central phenyl ring of the terphenyl backbone, avoiding thus dihydroindenofluorenyl isomers formation.[*] The synthetic approach starts with the oxidation of the methyl groups of 1,5-dibromo-2,4-dimethylbenzene **1** with potassium permanganate in *tert*-butyl alcohol providing the dicarboxylic acid **2** with 71 % yield. Esterification of **2** in a mixture of ethanol and methanesulfonic acid (MsOH) provides **3** (78 % yield), further involved in a Suzuki-Miyaura cross coupling ($Pd(PPh_3)_4$, K_2CO_3, THF/H_2O) with phenylboronic acid to give the *meta* terphenyl **4** (95 % yield) with the ester groups on the central phenyl ring and in *ortho* position of each phenyl unit. Finally, acid promoted (MsOH) intramolecular Friedel–Crafts acylation of **4** at high temperature (120°C) readily took place to give the diketone **(2,1-*b*)-IF(=O)$_2$** with 98 % yield.[†] It should be mentioned that **(2,1-*b*)-IF(=O)$_2$**

[*] Indeed, another synthetic approach based on the cyclization of a positional isomer of **4** (possessing the ester groups on the peripheral phenyl rings) has been also investigated in the course of this work (See details in ESI). This approach has led to a 1/1 mixture of dihydroindeno[1,2-*a*]fluorene **(1,2-*a*)-IF(=O)$_2$** and dihydroindeno[2,1-*b*]fluorene **(2,1-*b*)-IF(=O)$_2$**, unfortunately very difficult to separate by column chromatography.

[†] **(2,1-*b*)-IF(=O)$_2$** and dihydroindenofluorenones in general can not be purified by column chromatography due to the strong interactions with silica gel.

is soluble in common organic solvents and impressively more soluble than its (1,2-*b*) isomer previously reported in literature.[9,10]

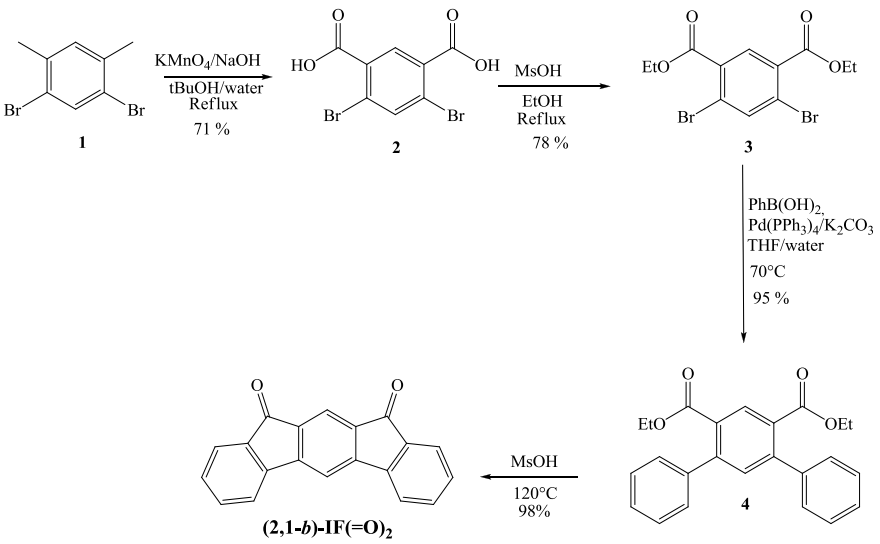

Scheme 2 Synthesis of **(2,1-*b*)-IF(=O)2**.

If the synthesis of **(2,1-*b*)-IF(=O)2** was straightforward, its conversion into its dicyanovinylene analogue **(2,1-*b*)-IF(=C(CN)2)2** appears to be a challenging task (Scheme 3). Indeed, the strong insolubility and the *syn* geometry of **(2,1-*b*)-IF(=C(CN)2)2** have significantly perturbed the efficiency of the Knoevenagel condensation used herein. Although similar reactions have been described for related molecules, such as dihydroindeno[1,2-*b*]fluorenone by Marks *et al*,[18] truxenone by Nielsen *et al*,[32] diindenopyrazinedione by Yamashita *et al*,[33] and pentaphenylenone by our group,[34] moderate to low yield reactions were reported due either to steric hindrance of the carbonyl units or to weak reactivity. In addition, the use of titanium tetrachloride, often used to activate the carbonyl units of sterically hindered molecules[18,32] only leads herein to degradation products, highlighting the instability of the dihydroindeno[2,1-*b*]fluorenyl core towards these harsh conditions.

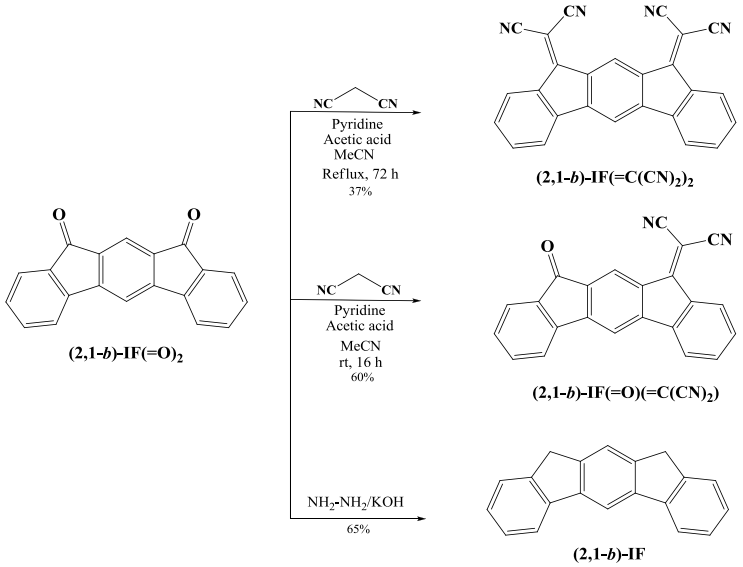

Scheme 3 Synthesis of **(2,1-*b*)-IF**, **(2,1-*b*)-IF(=O)(=C(CN)2)** and **(2,1-*b*)-IF(=C(CN)2)2.**

After intensive scouting (temperature, solvent, time of reaction, etc.), the best condensation procedure found was to reflux **(2,1-*b*)-IF(=O)2**, in acetonitrile for 3 days, with a large excess of malononitrile (37 % yield, see ESI for details). However, it is important to stress that **(2,1-*b*)-**

IF(=C(CN)$_2$)$_2$ is strongly insoluble in all the solvents tested rendering its analysis very complicated. In the course of optimization of this reaction, an interesting feature has been observed. Indeed, the incorporation of the first dicyanovinylene unit on **(2,1-*b*)-IF(=O)$_2$** occurs very quickly leading to the formation of **(2,1-*b*)-IF(=O)(=C(CN)$_2$)** bearing a dicyanovinylene unit and a ketone group, Scheme 3. Thus, Knoevenagel condensation of **(2,1-*b*)-IF(=O)$_2$** using exactly the same conditions than those described above but reducing the reaction time and temperature leads to the formation of (**2,1-*b*)-IF(=O)(=C(CN)$_2$)** with 60 % yield. The completion of the Knoevenagel condensation was supported by infrared spectroscopy (Figure S4 in ESI). It seems hence that the second condensation reaction appears difficult to perform. This finding correlates our above-mentioned hypothesis stating that the incorporation of bulky dicyanovinylene units on the dihydroindeno[2,1-*b*]fluorenyl core is difficult to perform due to steric hindrance induced by the *syn* geometry of the bridges. This feature has been confirmed by theoretical modelling since we unfortunately did not manage to grow crystals of neither (**2,1-*b*)-IF(=C(CN)$_2$)$_2$** nor **(2,1-*b*)-IF(=O)(=C(CN)$_2$)** (Figure 1). Thus, the more stable conformer obtained by theoretical modelling (DFT) for **(2,1-*b*)-IF(=C(CN)$_2$)$_2$** presents a tilt for the two dicyanovinylene bridges, one pointing above the dihydroindeno[2,1-*b*]fluorenyl plane (through the central phenyl ring) and the other pointing below this plane (Figure 1, top). In addition, the distance between the two closest nitrogen atoms of the dicyanovinylene units has been evaluated at ca 3.4 Å, close to the sum of the van der Waals radius (3 Å)[35] and the distance between the nitrogen atoms and the central hydrogen atom has been evaluated at 2.6 Å. This up/down structural feature found in the model of **(2,1-*b*)-IF(=C(CN)$_2$)$_2$** leads to a dihedral angle of ca 19.8° between the mean planes of the dicyanovinylenes and has been assigned to the steric hindrance induced by the presence of the two dicyanovinylene bridges on the same side of the dihydroindenofluorenyl core.[*] Such deformation has not been detected in the model of **(2,1-*b*)-IF(=O)(=C(CN)$_2$)**, the carbonyl and the dicyanovinylene unit being in an eclipsed conformation (Figure 1, bottom).

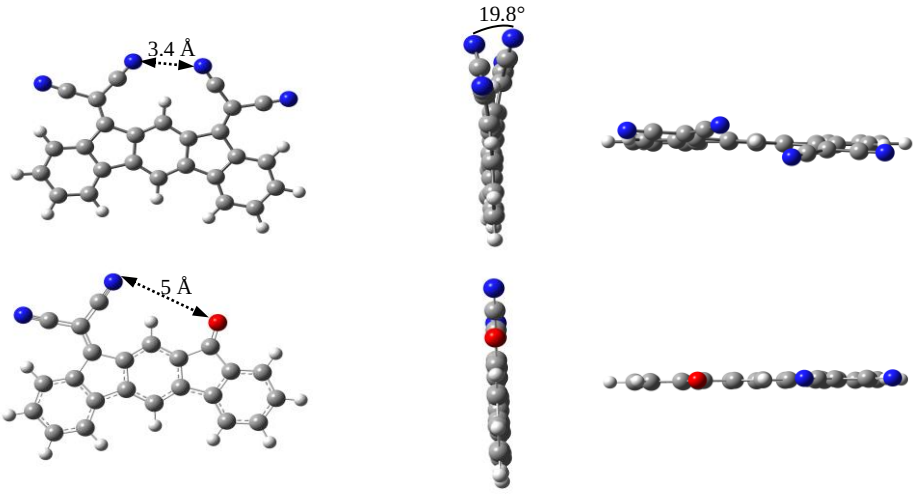

Figure 1 Different views of the more stable conformer obtained for (**2,1-*b*)-IF(=C(CN)$_2$)$_2$** (Top) and **(2,1-*b*)-IF(=O)(=C(CN)$_2$)** (Bottom) by DFT calculations.

Finally, reduction of key diketone **(2,1-*b*)-IF(=O)$_2$** in basic media through Wolff–Kishner conditions as previously described for other dihydroindenofluorene isomers[12] leads to **(2,1-*b*)-IF**, the simplest analogue in the series (Scheme 3).

[*] It should be noted that a similar up/down tilt has been observed in the crystal structure of structurally related dihydroindeno [1,2-*b*]- and [2,1-*a*]-fluorenes with spirofluorenes on the bridges (*Org. Lett.* 2008, **10**, 373.).

Electrochemical properties

The electrochemical behaviours were studied in CH_2Cl_2 using cyclic voltammetry, Figure 2. **(2,1-*b*)-IF** study was performed at 4×10^{-3} M. As the other compounds are only weakly soluble and present a strong tendency to adsorb on Al_2O_3 used to keep the electrolytic medium as dry as possible, the studies **(2,1-*b*)-IF(=O)$_2$**, **(2,1-*b*)-IF(=O)(=C(CN)$_2$)** and **(2,1-*b*)-IF(=C(CN)$_2$)$_2$** were performed in saturated solutions.

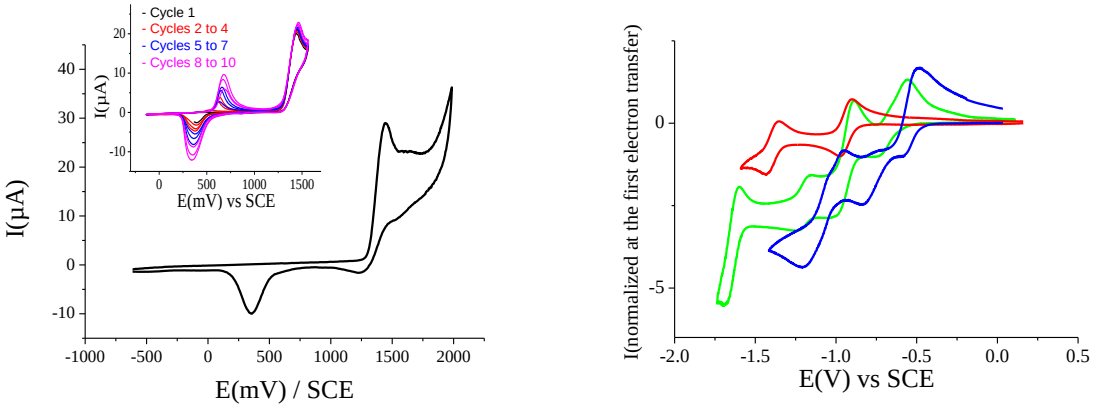

Figure 2 Cyclic voltammograms of **(2,1-b)-IF** in oxidation (left, inset: repeated potential sweeps) and of **(2,1-*b*)-IF(=C(CN)$_2$)$_2$** (green line), **(2,1-*b*)-IF(=O)$_2$** (red line) and **(2,1-*b*)-IF(=O)(=C(CN)$_2$)** (blue line), in reduction (right) recorded in CH_2Cl_2 (Bu_4NPF_6 0.2 M), working electrode: platinum disk diameter 0.25 mm, sweep-rate: 100 mV/s).

In oxidation (Figure 2, Left), **(2,1-*b*)-IF** presents an oxidation wave with a maximum recorded at 1.44 V and a threshold oxidation potential at 1.31 V. As shown in inset and contrary to both **(1,2-*b*)-IF**[36] and **(2,1-*a*)-IF**,[12] which first oxidation is reversible, **(2,1-*b*)-IF** is irreversibly oxidized at this first step. Repeated potential sweeps show the growth of a new redox system observed at less anodic potential and lead to the coverage of the electrode by an insoluble deposit. Such a behaviour signs the high reactivity of **(2,1-*b*)-IF** radical-cation which leads to carbon-carbon couplings and to anodic polymerization. This electropolymerization process occurs even more efficiently when the oxidation is performed to more anodic potentials (Figure S3 in ESI). The study of the electrochemical behaviour of a **poly((2,1-*b*)-IF**) modified electrode in absence of any electroactive molecule (see ESI) shows that the threshold oxidation potential of **poly((2,1-*b*)-IF**) is recorded at 0.245 V, that means 0.425 and 0.505 V less anodic than structurally related *para* syn bridged-terphenyl **poly((2,1-*a*)-IF**)[12] and *para* anti bridged-terphenyl **poly((1,2-*b*)-IF**)[36] respectively, showing a more extended conjugation in the present polymer. This features appears to be surprising as it is usually accepted that *para* linkages found in both **poly((1,2-*b*)-IF**) and **poly((2,1-*a*)-IF**) leads to longer π-conjugated pathways compared to *meta* linkages found in **poly((2,1-*b*)-IF**). The angle torsions between the constituting units may be the reason of this extended conjugation.

For the three other compounds, no distinct oxidation wave was observed before the oxidation of the electrolytic medium and it was only possible to record the onset potentials at 1.51, 1.53 and 1.50 V for **(2,1-*b*)-IF(=C(CN)$_2$)$_2$**, **(2,1-*b*)-IF(=O)$_2$** and **(2,1-*b*)-IF(=O)(=C(CN)$_2$)** respectively. Thus, in the anodic range, the difference between the two electron-withdrawing groups (carbonyl and dicyanovinylene units) appears to be extremely weak. However, these onset potential values are significantly more anodic (by more than 200 mV) than that of the non functionalized **(2,1-*b*)-IF** (1.31 V). This anodic shift is clearly indicative of the electron-withdrawing character of the ketone and dicyanovinylene units on the oxidation of the dihydroindenofluorenyl backbone. The same trend has been observed for bridged pentaphenylene derivatives.[34] HOMO levels lye at -5.91, -5.96 and -5.90 eV for **(2,1-*b*)-**

IF(=C(CN)$_2$)$_2$, **(2,1-*b*)-IF(=O)$_2$** and **(2,1-*b*)-IF(=O)(=C(CN)$_2$)** respectively, these values being almost identical but strongly deeper than that of **(2,1-*b*)-IF** (-5.71 eV).
In the cathodic range, **(2,1-*b*)-IF** presents no distinct reduction wave before the reduction of the electrolytic medium and it was only possible to record its onset potential at -2.36 V (See ESI). On the other hand, **(2,1-*b*)-IF(=O)$_2$** reduction occurs in two successive reversible reduction waves with maxima at -0.98 and -1.45 V, assigned to the reduction of the diketone to the quinonoid dianion.[17,18,37] The reduction of **(2,1-*b*)-IF(=C(CN)$_2$)$_2$** occurs in four reduction waves with maxima at -0.71, -1.00, -1.24 and -1.69 V. A dissymmetry of the molecule linked to a possible tilt of the bridgeheads might be responsible of this surprising feature. The first reduction wave of **(2,1-*b*)-IF(=C(CN)$_2$)$_2$** is positively shifted by 0.27 V compared to that of **(2,1-*b*)-IF(=O)$_2$** (Figure 2). In this case, and oppositely to the above conclusions in oxidation, this potential difference clearly indicates the stronger electron- withdrawing character of the dicyanovinylenes compared to that of the carbonyls. In addition, compared to **(2,1-*b*)-IF**, the substitution with cyanovinylenes in **(2,1-*b*)-IF(=C(CN)$_2$)$_2$** renders the reduction easier by 1.7 V, highlighting the efficiency of the design.
The reduction of **(2,1-*b*)-IF(=O)(=C(CN)$_2$)** occurs in three reduction waves with maxima at -0.59, -0.83 and -1.2 V. Surprisingly, the first reduction appears then even easier than the first reduction of **(2,1-*b*)-IF(=C(CN)$_2$)$_2$** (-0.59 V vs -0.71 V). Such an unexpected behaviour, which can be tentatively assigned to a possible deformation (induced by the steric hindrance) of **(2,1-*b*)-IF(=C(CN)$_2$)$_2$** or to electronic repulsion between the adjacent cyano groups is still under investigation in our group. The onset reduction potentials were pointed out at -0.59, -0.88 and -0.47 V for **(2,1-*b*)-IF(=C(CN)$_2$)$_2$**, **(2,1-*b*)-IF(=O)$_2$** and (**2,1-*b*)-IF(=O)(=C(CN)$_2$)** respectively leading to LUMO levels lying at -3.81, -3.52 and -3.93 eV. These energy levels are remarkably lower than that of **(2,1-*b*)-IF** (-2.04 eV). Thus, the LUMO energy of the substituted compounds is impressively more affected by the substitution (maximum shift reaching 1.89 eV) than the HOMO energy (maximum shift of 0.2 eV, see above). This suggests that the LUMOs are localized on the bridges, rendering these LUMO levels more sensitive to bridges functionalization. Oppositely, the HOMOs seem to be more delocalized over the dihydroindenofluorenyl core and are hence less sensitive to bridges functionalization. This finding, confirmed through theoretical calculations (Figure 3), indicates that the present design allows selectively tuning the LUMO energy levels with only a weak alteration of their HOMO levels. The electrochemical gap Eg^{el} of (**2,1-*b*)-IF(=O)$_2$** (2.44 eV), of **(2,1-*b*)-IF(=O)(=C(CN)$_2$** (1.97 eV) and of **(2,1-*b*)-IF(=C(CN)$_2$)$_2$** (2.1 eV) are therefore largely lower than that of **(2,1-*b*)-IF** (3.67 eV), Table 1.

Table 1 Electronic properties of **(2,1-*b*)-IF**, **(2,1-*b*)-IF(=O)$_2$**, **(2,1-*b*)-IF(=O)(=C(CN)$_2$)** and **(2,1-*b*)-IF(=C(CN)$_2$)$_2$**

	E^1_{ox} (V)[a]	E^{onset}_{ox} (V)[a]	E^1_{red} (V)[a]	E^2_{red} (V)[a]	E^{onset}_{red} (V)[a]	LUMO (eV)[b]	HOMO (eV)[b]	Eg^{el} (eV)[c]	LUMO (eV)[d]	HOMO (eV)[d]	Eg^{theo} (eV)[d]
(2,1-*b*)-IF	1.44	1.31	-	-	-2.36	-2.04	-5.71	3.67	-1.29	-5.82	4.53
(2,1-*b*)-IF(=O)$_2$	Not observable	1.56	-0.98	-1.45	-0.88	-3.52	-5.96	2.44	-3.18	-6.59	3.41
(2,1-*b*)-IF(=O)(=C(CN)$_2$)	Not observable	1.50	-0.59	-0.83 -1.20	-0.47	-3.93	-5.90	1.97	-3.79	-6.79	3.00
(2,1-*b*)-IF(=C(CN)$_2$)$_2$	Not observable	1.51	-0.71	-1.00 -1.24 -1.69	-0.59	-3.81	-5.91	2.10	-4.05	-6.96	2.91

[a] *vs* SCE; [b] calculated from onset oxidation/reduction potential taken from CV (Fig. 2); [c] from electrochemical data Eg^{el}=HOMO-LUMO; [d] from theoretical calculations.

The HOMO of the four compounds is dispersed on the dihydroindeno[2,1-*b*]fluorenyl core, highlighting that the substitution on the bridgeheads with electron-withdrawing fragments do

not disturb the character of the HOMO (Figure 3, Bottom). Thus, the bridges are not directly involved in the HOMO character of the four compounds and this feature explains the small energy modulation observed through electrochemical experiments between the three substituted compounds, ie **(2,1-*b*)-IF(=O)$_2$**, **(2,1-*b*)-IF(=O)(=C(CN)$_2$)** and **(2,1-*b*)-IF(=C(CN)$_2$)$_2$**. Thus, the presence of electron-withdrawing groups on the bridgeheads despite not disturbing the character of the HOMO has nevertheless an influence on the HOMO energy level of **(2,1-*b*)-IF** (see above). Oppositely, the localisation of the LUMO appears to be different and sensitive to the bridge substitution. Indeed, **(2,1-*b*)-IF** possesses a LUMO mainly dispersed on the central phenyl ring with no density on the bridge. The incorporation of ketones on the bridgeheads of **(2,1-*b*)-IF(=O)$_2$** leads to a LUMO mainly localised on the two cyclopentadienones. Introducing dicyanovinylene units leads to a shift of the LUMO localisation from cyclopentadienone in **(2,1-*b*)-IF(=O)$_2$** to cyclopentadiene/dicyanovinylene in **(2,1-*b*)-IF(=O)(=C(CN)$_2$)** (one dicyanovinylene) and **(2,1-*b*)-IF(=C(CN)$_2$)$_2$** (two dicyanovinylenes). This is directly linked to the electron-withdrawing strength of dicyanovinylene compared to carbonyl. These results are in accordance with the assignment of the different electron transfers presented in the electrochemical part and clearly show why the LUMO levels are strongly more influenced by the bridges than the HOMO levels are.

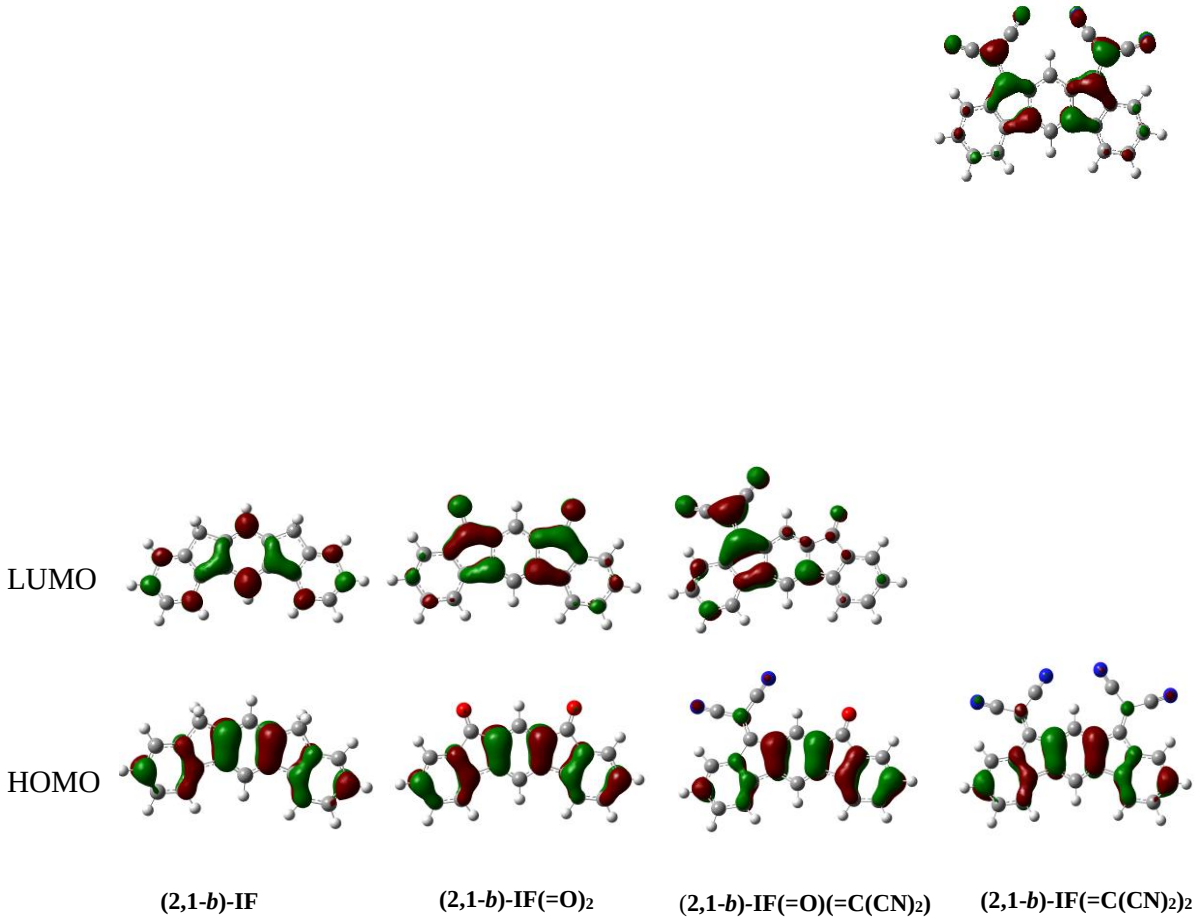

Figure 3 Sketch of frontier molecular orbitals (isovalue: 0.04 [e bohr^{-3}]$^{1/2}$) of **(2,1-*b*)-IF**, **(2,1-*b*)-IF(=O)$_2$**, **(2,1-*b*)-IF(=O)(=C(CN)$_2$)** and **(2,1-*b*)-IF(=C(CN)$_2$)$_2$** from DFT calculations.

UV-Vis absorption spectra

UV-Vis absorption spectra of the four dyes in THF solution are shown in Figure 4 and optical data are collected in Table 2.

(2,1-*b*)-IF (Figure 4 left, black line) presents a very well resolved spectrum with a fine vibronic structure reflecting a very rigid molecular structure. The absorption maximum is recorded at 332 nm, leading to an optical gap Eg^{opt} of 3.62 eV. This band at 332 nm corresponds, in the light of Time Dependant-DFT (TD-DFT) calculations (see below), to an HOMO/LUMO transition (π–π*) with both orbital delocalized on the dihydroindeno[2,1-*b*]fluorenyl core (Figure 5, Top-left). This transition presents a large oscillator strength (f = 0.2621, λ= 313 nm) in accordance with the molar extinction coefficient (17640 $L.mol^{-1}.cm^{-1}$) calculated at 332 nm from the UV-Vis absorption spectrum (Figure 4). Similar behaviour has been recently observed for *para*-susbituted dihydroindenofluorene isomers **(1,2-*b*)-IF** and **(2,1-*a*)-IF** (See structures in ESI).[12]

The absorption maximum of **(2,1-*b*)-IF** is slightly blue shifted (2 nm) compared to that of its *para*-substituted *anti* isomer **(1,2-*b*)-IF** (λ = 334 nm in decalin, Eg^{opt} = 3.61 eV)[12] but significantly red shifted (10 nm) compared to the other *syn para*-substituted isomer **(2,1-*a*)-IF** (λ = 322 nm in THF, Eg^{opt} = 3.76 eV).[12] Thus, we note that despite different phenyl linkages, *meta* in **(2,1-*b*)-IF**, and *para* in **(1,2-*b*)-IF**, Eg^{opt} is identical, indicating that the geometry of the π–conjugated core has a significant influence on the π-electrons delocalization and may be even more important than the nature of the linkages.[30,31] This is confirmed with the constrained *syn* structure of **(2,1-*a*)-IF**, which presents the most blue-shifted maximum, 322 nm (and the most contracted Eg^{opt}=3.76 eV) in the series, reflecting therefore a poor delocalization of π-electrons. These features highlight the importance of the linkages (*meta vs para*) but also of the geometry (*syn vs anti*) on the conjugation pathways.[30,31]

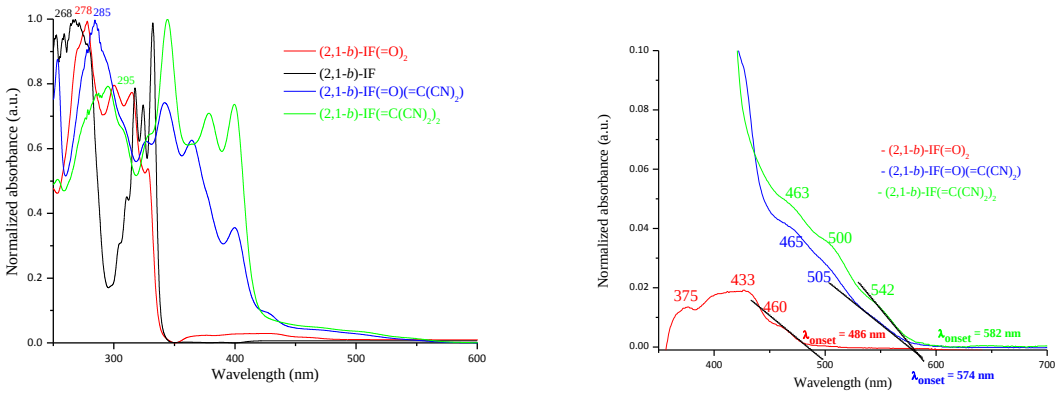

Figure 4 Left: Normalized UV-Vis spectra of **(2,1-*b*)-IF** (black line) **(2,1-*b*)-IF(=O)$_2$** (red line), **(2,1-*b*)-IF(=O)(=C(CN)$_2$)** (blue line) and **(2,1-*b*)-IF(=C(CN)$_2$)$_2$** (green line), in THF, Right: Focus on the 350/700 nm portion of the spectra.

Table 2. Optical properties of **(2,1-*b*)-IF**, **(2,1-*b*)-IF(=O)$_2$**, **(2,1-*b*)-IF(=O)(=C(CN)$_2$)** and **(2,1-*b*)-IF(=C(CN)$_2$)$_2$.**

	λ_{abs} (nm)	Eg^{opt} (eV)[a]
(2,1-*b*)-IF	268, 304, 311, 318, 324, 332	3.62
(2,1-*b*)-IF(=O)$_2$	278, 300, 315, 328, 375, 433, 460 (sh)	2.55
(2,1-*b*)-IF(=O)(=C(CN)$_2$	285, 306 (sh), 326, 342, 363, 400, 427, 465 (sh), 505 (sh)	2.16
(2,1-*b*)-IF(=C(CN)$_2$)$_2$	295, 306 (sh), 329, 344, 378, 400, 463 (sh), 500 (sh), 542 (sh)	2.13

[a] Eg^{opt} [eV]=hc/λ, λ being the low energy absorption band edge (in meter, see Figure 4, Right), with h = 6.62606×10^{-34} J.s (1eV=1.60217×10^{-19} J) and c =2.99792×10^{8} $m.s^{-1}$, Eg^{opt} (eV) = 1239.84 / λ (in nm).

(**2,1-*b*)-IF(=O)$_2$** also presents a well resolved absorption spectrum with maxima at λ = 278, 300, 315 and 328 nm (Figure 4, Left, red line), similar to those of (**2,1-*b*)-IF** and hence assigned to π−π* transitions. The same trend has been observed between a pentaphenylene and its corresponding diketone.[34] A weak and broad absorption band was also observed at lower energy between 350 and 500 nm (Figure 4, Right). This transition possesses a weak molar extinction coefficient ($\varepsilon_{433\ nm} \sim 0.05 \times 10^4$ L.mol^{-1}.cm^{-1}) in accordance with the weak oscillator strength (f = 0.0055, Figure 5, Top-right) and has been assigned to a HOMO/LUMO transition.[34,37-39,40] As the HOMO is dispersed on the dihydroindenofluorenyl core and the LUMO on the cyclopentadienone unit, this transition presents a charge transfer character. In addition, the transition possessing the largest oscillator strength (λ = 329 nm, f = 0.4432 nm)* involves a HOMO/LUMO+1 transition (38 %) and a HOMO-1/LUMO transition (45 %). Since the HOMO (-6.59 eV), LUMO (-3.18 eV) and LUMO+1 (-2.49 eV) are the highest in the series (and considering as well that the HOMO-1 energy level is identical to those of the other molecules), it explains the blue shift observed in the main absorption bands of (**2,1-*b*)-IF(=O)$_2$** compared to those of its dicyanovinylene analogues (see below).

(**2,1-*b*)-IF(=O)(=C(CN)$_2$)** presents four main bands at 285, 342, 363 and 400 nm and a shoulder at 427 nm, red shifted compared to those of (**2,1-*b*)-IF(=O)$_2$**, due to extended conjugation induced by the incorporation of one dicyanovinylene unit (Figure 4, blue line). The HOMO/LUMO transition of **(2,1-*b*)-IF(=O)(=C(CN)$_2$)** (Figure 5, Bottom-left) presents a weak oscillator strength (f = 0.0267), the HOMO being dispersed on the dihydroindenofluorene and the LUMO on the cyclopentadiene/dicyanovinylene. Thus, the localization of the LUMO of **(2,1-*b*)-IF(=O)(=C(CN)$_2$)** is different to that of (**2,1-*b*)-IF(=O)$_2$** whereas both LUMO+1 are similar. This is an important characteristic of **(2,1-*b*)-IF(=O)(=C(CN)$_2$)** and for the excited states considered,* we note that the main transition (f = 0.4748, λ = 367 nm) contains HOMO-1/LUMO (38 %) and HOMO/LUMO+1 (58 %) contributions. The HOMO/LUMO+1 transition is hence the main transition in both (**2,1-*b*)-IF(=O)$_2$** and **(2,1-*b*)-IF(=O)(=C(CN)$_2$)** with the same molecular fragments involved for both molecules (HOMO: dihydronindenofluorene / LUMO+1 : cyclopentadienone).

UV-Vis absorption spectrum of **(2,1-*b*)-IF(=C(CN)$_2$)$_2$** presents four main bands with maxima at 295, 344, 378 and 400 nm (Figure 4, green line). A very weak and broad absorption is also detected at low energy (above 450 nm, Figure 4, Right), assigned to a HOMO/LUMO transition possessing a weak oscillator strength (f = 0.0175, Figure 5, Bottom-right). In addition, the main transitions are (i) a HOMO-1/LUMO (53 %, f = 0.4564, λ = 406 nm) and a HOMO/LUMO+1 (47 %, f = 0.4564, λ = 406 nm) and (ii) a HOMO-1/LUMO+1 (f = 0.4753, 56 %, λ = 349 nm). Thus, we note that in the three last transitions (344, 378 and 400 nm for **(2,1-*b*)-IF(=C(CN)$_2$)$_2$** and 342, 363 and 400 nm for **(2,1-*b*)-IF(=O)(=C(CN)$_2$)**) two are recorded at almost identical wavelengths (342 vs 344 nm and 400 vs 400 nm, Table 2), whereas one is significantly red shifted by 15 nm in the case of **(2,1-*b*)-IF(=C(CN)$_2$)$_2$** (363 *vs* 378 nm). This transition surely involves the dicyanovinylene functions for **(2,1-*b*)-IF(=C(CN)$_2$)$_2$** and the carbonyl function for **(2,1-*b*)-IF(=O)(=C(CN)$_2$)** and is therefore assigned to a HOMO-LUMO+1 transition. Indeed, we note that in both **(2,1-*b*)-IF(=O)(=C(CN)$_2$)** and **(2,1-*b*)-IF(=C(CN)$_2$)$_2$**, the LUMO+1 is always implicated in the transitions with the largest oscillator strength but is dispersed on different fragments (cyclopentadienone for **(2,1-*b*)-IF(=O)(=C(CN)$_2$)** and cyclopentadiene/dicyanovinylene for **(2,1-*b*)-IF(=C(CN)$_2$)$_2$**), leading to an impressive energy difference (-2.89 eV for **(2,1-*b*)-IF(=O)(=C(CN)$_2$)** and -3.50 eV for **(2,1-*b*)-IF(=C(CN)$_2$)$_2$**)).†

* With λ> 300 nm

† It should be mentioned that the trend is perfectly followed as the LUMO of (**2,1-*b*)-IF(=O)$_2$** lies at -2.49 eV.

On the contrary, HOMOs of **(2,1-*b*)-IF(=O)(=C(CN)$_2$)** and **(2,1-*b*)-IF(=C(CN)$_2$)$_2$**) lie at close energy levels (-6.79 eV *vs* -6.96 eV respectively) and their HOMO-1 even lie at the same energy level (7.26 eV *vs* 7.27 eV respectively). This may explain the difference observed between some bands in their experimental absorption spectra. Thus, the bathochromic shift upon dicyanovinylene functionalization is mainly attributed to the decrease of the LUMO level due to the stronger electron-withdrawing nature of the dicyanovinylene compared to the carbonyl,[16,17,34,40] resulting in an optical gap Eg^{opt} * contraction from 2.55 eV for **(2,1-*b*)-IF(=O)$_2$** to 2.16 eV for **(2,1-*b*)-IF(=O)(=C(CN)$_2$)** and to 2.13 eV for **(2,1-*b*)-IF(=C(CN)$_2$)$_2$**, Table 1. These energy gaps are impressively contracted (by more than 1.5 eV) compared to that of **(2,1-*b*)-IF** (3.62 eV) due to HOMO/LUMO decrease with a more important magnitude in the latter (see above).

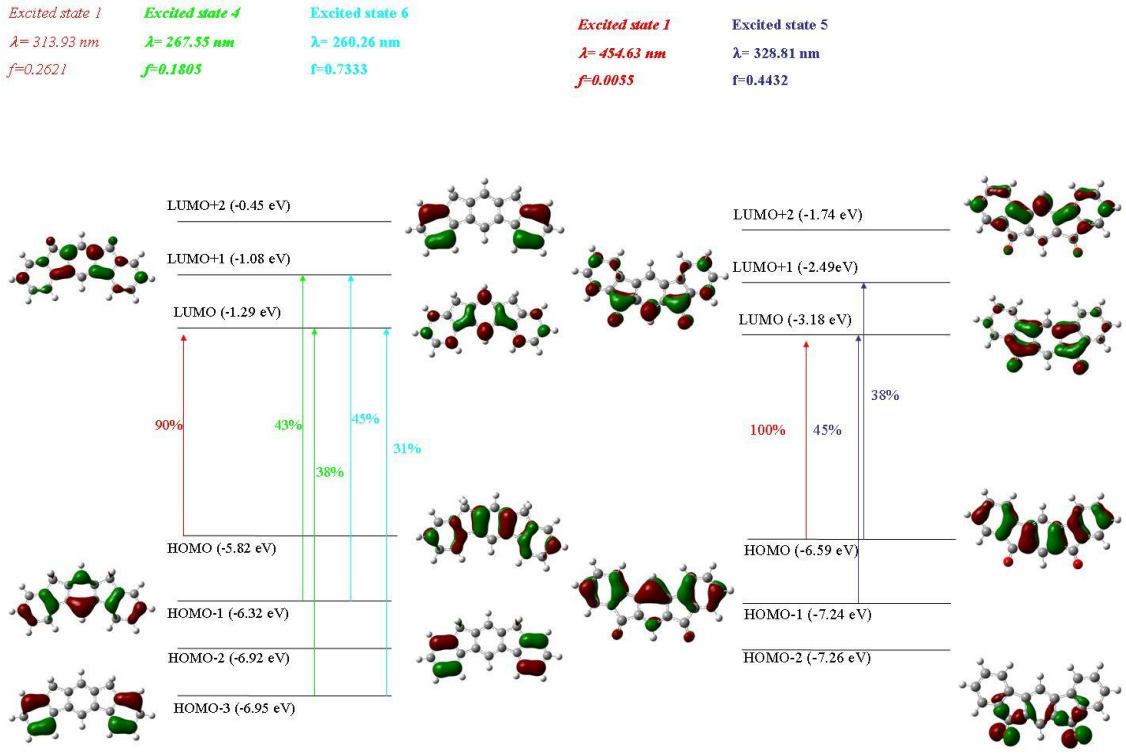

* As depicted below, TD-DFT calculations have allowed assigning the low energy band in (**2,1-*b*)-IF(=O)$_2$**, **(2,1-*b*)-IF(=O)(=C(CN)$_2$)** and **(2,1-*b*)-IF(=C(CN)$_2$)$_2$** to an HOMO/LUMO transition.

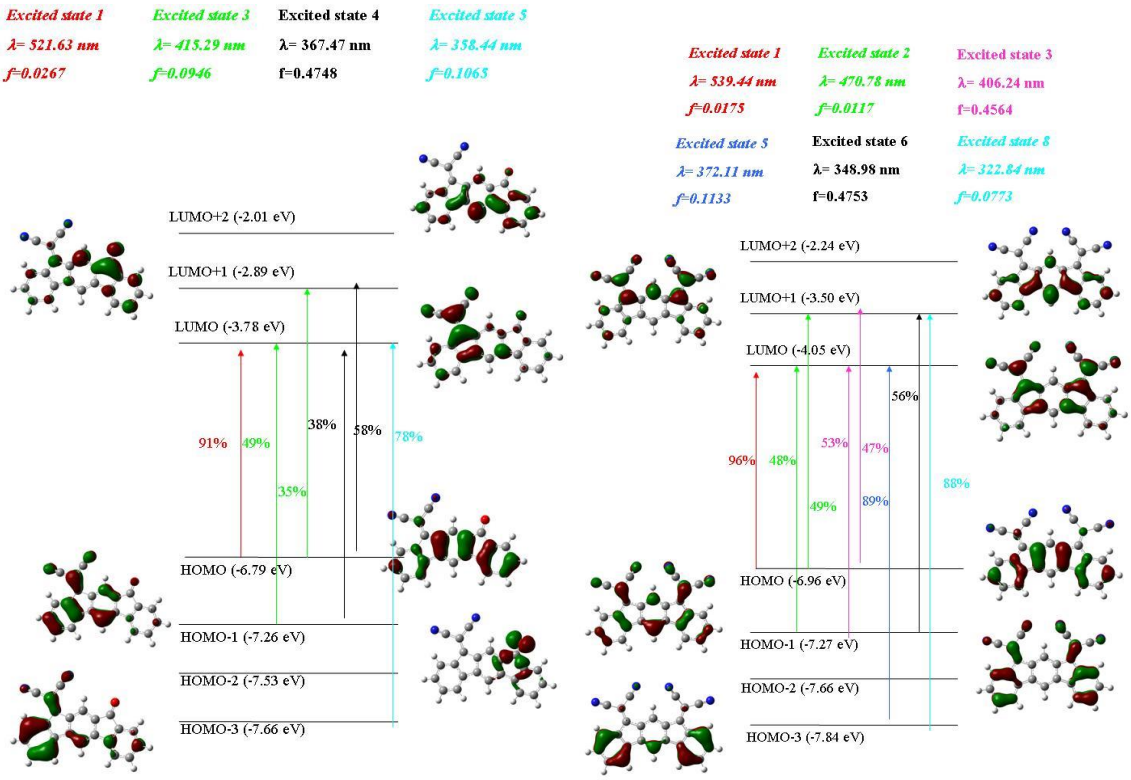

Figure 5 Sketch of calculated frontier molecular orbitals by DFT and the first calculated electronic transitions by TD-DFT of (**2,1-*b*)-IF** (top left), **(2,1-*b*)-IF(=O)$_2$** (top right), **(2,1-*b*)-IF(=O)(=C(CN)$_2$)** (bottom left) and **(2,1-*b*)-IF(=C(CN)$_2$)$_2$** (bottom right), after geometry optimization with DFT B3LYP/6-311G+(d,p), shown with a cut-off 0.04 [e bohr^{-3}]$^{1/2}$.

Fluorescence Spectroscopy

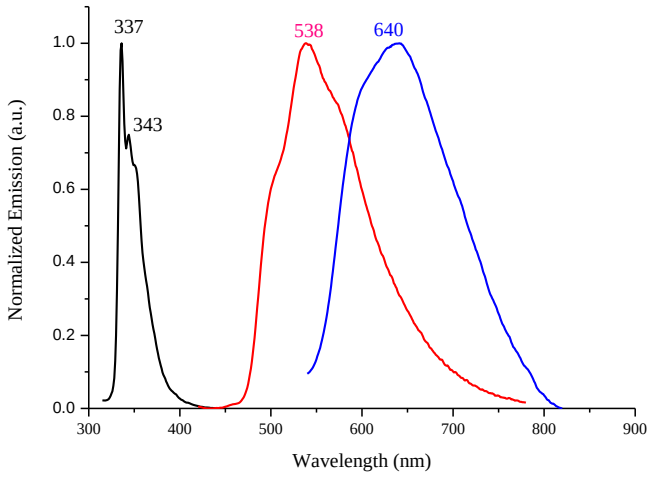

Figure 6 Normalized Fluorescence spectra in THF of **(2,1-*b*)-IF** (black line, λ_{exc} =300 nm) **(2,1-*b*)-IF(=O)$_2$** (red line) and **(2,1-*b*)-IF(=O)(=C(CN)$_2$)** (blue line, λ_{exc} =400 nm). Normalization was performed at λ_{max} in the 300 nm to 850 nm range.

The fluorescence spectrum of **(2,1-*b*)-IF** in THF presents a fine vibronic structure with two maxima at 337 nm and 343 nm (Figure 6, black line). As previously observed for other

dihydroindenofluorenes **(1,2-*b*)-IF** and **(2,1-*a*)-IF**,[9,12,27] **(2,1-*b*)-IF** is an efficient violet emitter possessing a high quantum yield in solution (ca 0.5, compared to quinine sulphate) and may hence be used to design highly efficient semi-conductors (oligomers or polymers) for OLEDs applications.[30] The fluorescence spectrum of **(2,1-*b*)-IF(=O)$_2$** is drastically different with a broad band of weak intensity centred at 538 nm (Figure 6, red line). Thus, the incorporation of oxygen atoms in the dihydroindeno[2,1-*b*]fluorenyl core leads not only to an impressive shift of the maxima compared to **(2,1-*b*)-IF** and also to an impressive decrease of the fluorescence intensity. **(2,1-*b*)-IF(=O)(=C(CN)$_2$)** also presents a weak fluorescence with a broad band centred at 640 nm. The shift of the main band from 538 nm for **(2,1-*b*)-IF(=O)$_2$** to 640 nm for **(2,1-*b*)-IF(=O)(=C(CN)$_2$)** may be due, in part, to the extended conjugation induced by the incorporation of the dicyanovinylene functionality. Finally, in the different solvent tested, **(2,1-*b*)-IF(=C(CN)$_2$)$_2$** displays no significant fluorescence (or too weak to be properly mentioned). A similar emission quenching has been previously assigned for related structures to non-radiative internal energy/electron transfers between the π–conjugated core and the dicyanovinylene units before emission.[17]

Organic Field Effect Transistors

The potential of **(2,1-*b*)-IF(=O)$_2$**, **(2,1-*b*)-IF(=O)(=C(CN)$_2$)** and **(2,1-*b*)-IF(=C(CN)$_2$)$_2$** as active layer of n-channel OFETs has been estimated through the fabrication and the electrical characterization of n-type OFETs with a Bottom Gate-Bottom Contacts structure (Figure 7). The electrical properties of OFETs were extracted under nitrogen atmosphere from transfer and output characteristics (Figure 7). The most important parameters are (i) the mobility μ_{FE} linked to the frequency operation in CMOS devices, (ii) the threshold voltage V_{TH} that determines the working voltage of OFET and (iii) on/off values of the drain – source resistance R_{DS} linked to the on and off status of a FET in CMOS circuits. The mobility is extracted from the linear and the saturated regime. The values obtained in both cases are in the same magnitude order and are reported in the Table 3.

First, no field effect is detected for the OFETs using **(2,1-*b*)-IF(=O)$_2$** as active layer. The incorporation of a dicyanovinylene unit in **(2,1-*b*)-IF(=O)(=C(CN)$_2$)** allows to reach a modest mobility of 4.6×10^{-6} cm²/V.s with a threshold voltage of 18.4 V, a subthreshold slope SS=5.74V/dec and a I_{on}/I_{off} =10^3-10^4 (Table 3). Despite low, the performance of **(2,1-*b*)-IF(=O)(=C(CN)$_2$)**, clearly highlights the impressive effect of the integration of one dicyanovinylene unit on the dihydroindeno[2,1-*b*]fluorenyl core. **(2,1-*b*)-IF(=C(CN)$_2$)$_2$** exhibit the best results in the series with a field effect mobility of ca 1×10^{-3} cm²/V.s, a low threshold voltage of 7.2 V and a subthreshold slope (SS) of 2.16 V/dec. These results are undoubtedly sufficient to realize such OFETs integrated in more complex circuits, which is a key point for the future of organic electronic. Indeed, and although the mobility, the subthreshold slope, the threshold voltage and the I_{on}/I_{off} ratio provide interesting information to compare organic semi-conductors in an OFET, they are not sufficient to perfectly understand their behaviour in a circuit. Thus, it is important to know, what occur in the active layer under polarization and in the interface between the insulator and the active layer. Indeed and as stated in the introduction, the main problem to achieve a circuit based on organic layers is the electrical instability.[40] Previous works have tried to address this key feature through the comparison of organic transistors with well known silicon-based devices.[41-43]

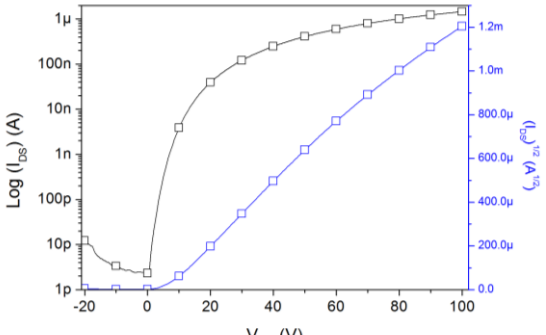

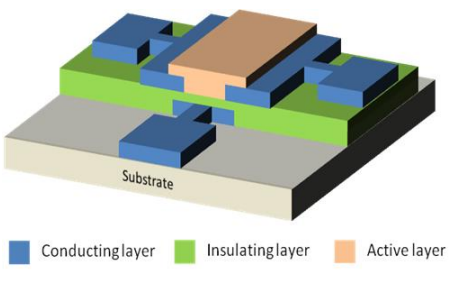

Figure 7 Transfer characteristics of OFET with **(2,1-*b*)-IF(=C(CN)$_2$)$_2$** as active layer and W/L=1000µm/5µm.

Table 3. Selected Electrical properties

Organic semiconductor	Threshold voltage V_{TH} (V)	Subthreshold swing S (V/dec)	Field effect mobility μ_{EF} $cm^2/V.s$	I_{DSON}/I_{DSOFF}
(2,1-*b*)-IF(=C(CN)$_2$)$_2$	7.2	2.16	1.02×10^{-3}	6.3×10^{5}
(2,1-*b*)-IF(=O)(=C(CN)$_2$)	18.4	5.74	4.6×10^{-6}	10^3-10^4
(2,1-*b*)-IF(=O)$_2$	No field effect			

A gate bias stress is employed herein to estimate the electrical (in)stability of **(2,1-*b*)-IF(=C(CN)$_2$)$_2$** based OFETs. The threshold voltage shift was evaluated by measuring transfer characteristics (I_D vs. V_{GS}) from V_{GS}=-20 V to V_{GS}=100 V every 10 minutes. Between two measurements, constant voltages were applied on gate electrode and on drain electrode (V_{DS}= 0 V). The drain and source electrodes were grounded to stress uniformly the TFT channel. Thus, the shifts of these electrical parameters, namely threshold voltage V_{TH}, subthreshold slope S and field effect mobility μ_{FE} under gate bias stress have been precisely investigated in order to shed light on the electrical (in)stability of **(2,1-*b*)-IF(=C(CN)$_2$)$_2$** based OFETs.

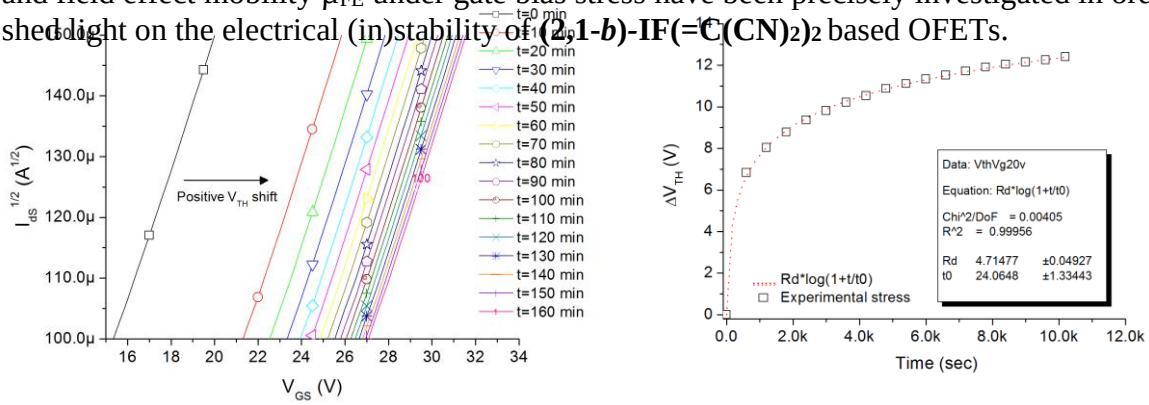

Figure 8 Study of V_{TH} shift under gate bias stress

First, regarding the evolution of V_{TH} under gate bias stress (10V, 20V, 30V and 40V), we note that the V_{TH} shifts are always the same following a logarithmic evolution according to stress time (Figure 8). The relation (1) obtained from the gate bias stress for ΔV_{TH} indicates that the instability of the devices is only related to charges trapping into the insulator and not into the active layer of **(2,1-*b*)-IF(=C(CN)$_2$)$_2$** itself. Assuming that the threshold voltage shift is due to trapped charges, the electric field created by these charges has to be compensated by the gate bias before an accumulation layer can be formed. Similar behaviours have already been observed in amorphous silicon TFT[6] for high gate voltage and in some cases in OFET.[44,45]

$$\Delta V_{TH} = R_D \log\left(1+\frac{t}{t_0}\right) \qquad (1)$$

Where R_D is a constant related to the density of traps N_t (cm^{-3}) in the insulator and the tunnelling constant λ (cm).

Additionally, the subthreshold slope related to defect in the interface between semiconducting layer and insulating layer is almost constant under gate bias stress, which indicates that no defect state have been created in this interface. From the subthreshold slope value, the density of defect state N_{it} at this interface has been estimated to be around 2.52×10^{12} cm². This value is very low and could be even compared to the best values reported to date for organic transistors. For example, Kippelen and coworkers have reported a N_{it} of ca 10^{12} cm² for a C60 based OFET,[46] highlighting herein the potential of **(2,1-*b*)-IF(=C(CN)₂)₂**.

Finally, the mobility μ_{FE} of **(2,1-*b*)-IF(=C(CN)₂)₂** also appears to be constant under applied stress (Figure 9). One can hence conclude that no defect has been created in the organic semiconducting layer of the OFET. This is an important characteristic, which directly translates the efficiency and stability of **(2,1-*b*)-IF(=C(CN)₂)₂**.

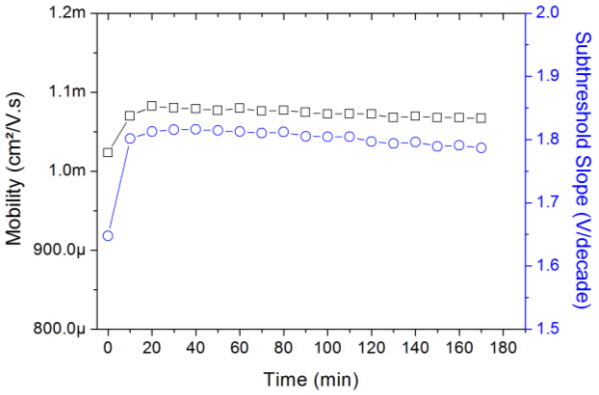

Figure 9 Mobility and Subthreshold Swing Vs stress time (V_{GSbias}=20V, V_{DS}=0V)

In summary, **(2,1-*b*)-IF(=C(CN)₂)₂** based OFETs present under gate bias stress a constant mobility and a constant subthreshold swing. In addition, the threshold voltage shift is characteristic of charges trapping mechanism into the insulator and not into the semi-conductor **(2,1-*b*)-IF(=C(CN)₂)**. The electrical stability of the OFETs is hence highly promising and allow their incorporation in an integrated circuit.

Finally, as a proof of concept, pseudo CMOS inverters[47] made of n-type **(2,1-*b*)-IF(=C(CN)₂)₂**-based OFETs have been fabricated and characterized (Figure 10). The response efficiency of logic gate as inverter is related to on/off states of p type and n type OFET. The on/off states are defined by the R_{DSon} and R_{DSoff} ratio corresponding to the (I_{DS},V_{DS}) slope (Figure 11). It should be mentioned that these preliminary works have been performed with n-type OFETs and using active charges instead of p-type OFETs. In a typical circuit, the OFETs switch from the saturated regime to the linear regime. The ability of a device to switch is directly linked to the difference between linear R_{DS} (R_{DSon}) and saturated R_{DS} (R_{DSoff}), Figure 10. Thus, the R_{DSon}/R_{DSoff} ratio (extracted from the output characteristics) is hence a key parameter in a circuit.* Herein, the R_{DSoff}/R_{DSon} ratio is evaluated at 1.5×10^{3}, this value being significantly high to well discriminate the off and the on state.

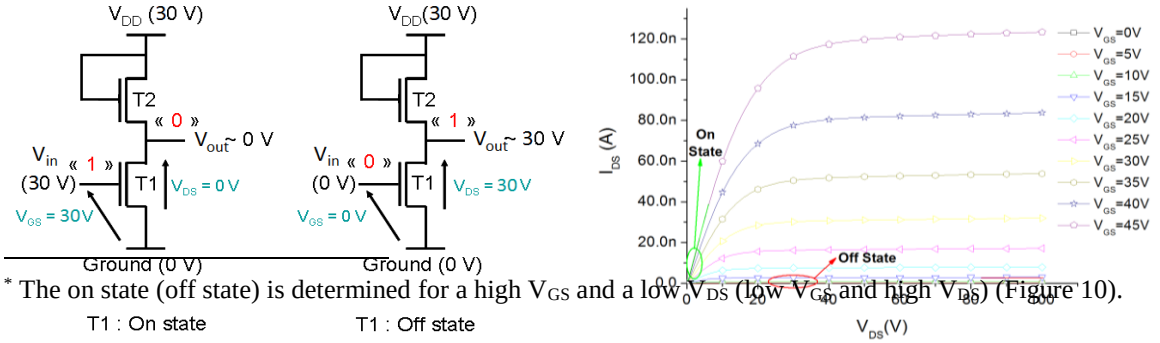

* The on state (off state) is determined for a high V_{GS} and a low V_{DS} (low V_{GS} and high V_{DS}) (Figure 10).

Figure 10. Schematic of Pseudo CMOS inverter and T1 associated output characteristics

Pseudo CMOS inverters have been electrically characterized with a 10 Hz square signal applied as input voltage (V_{in}). We observe that output voltage V_{out} follows a classical inverter behaviour with a high value about 27.5 V when V_{in}=0V and a low value about 0.5 V when V_{in}=30V (figure 11). In addition, we note that for a V_{DD} of 30 V, the V_{out} is measured at ca 27.5V, which is promising for embedded circuits. This first result allows hence to observe OFET made of **(2,1-*b*)-IF(=C(CN)$_2$)$_2$** under real polarization conditions and no degradation of on and off voltage for V_{out} have been observed with a continuous 12 hours polarization.

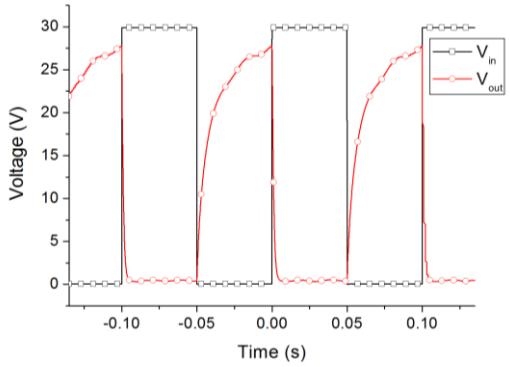

Figure 11. Inverter made of n-type **(2,1-*b*)-IF(=C(CN)$_2$)$_2$** OFETs with W/L=1000/2 and 250/20 for the active charge.

Conclusion

In summary, we report herein a complete structure properties relationship study of bridged *syn* triphenylene derivatives, namely 5,7-dihydroindeno[2,1-*b*]fluorene, functionalized on the bridgeheads with methylenes, **(2,1-*b*)-IF**, carbonyls, **(2,1-*b*)-IF(=O)$_2$**, both carbonyl and dicyanovinylene, **(2,1-*b*)-IF(=O)(=C(CN)$_2$)** and dicyanovinylene units **(2,1-*b*)-IF(=C(CN)$_2$)$_2$**. This latter compounds which possesses a very low LUMO level, ca -3.81 eV, has been successfully used as active layer in n-channel OFETs using epoxy based photoresist SU-8 as gate insulator. **(2,1-*b*)-IF(=C(CN)$_2$)$_2$** based n-channel OFETs present an electron mobility of 10^{-3} cm²/V.s and show very promising properties such as low voltage functioning of 7.2 V (low gate-source and drain-source voltages), high ratio between the on and the off currents (6.3×10^5) interesting subthreshold swing (SS=2.16) and electron mobility ($>10^{-3}$ cm^2/V.s) and more importantly excellent stability under electrical stress. This electrical stability has allowed to incorporate **(2,1-*b*)-IF(=C(CN)$_2$)$_2$** based n-channel OFETs in an integrated circuit. Thus, pseudo CMOS inverters made of n-type **(2,1-*b*)-IF(=C(CN)$_2$)$_2$**-based OFETs (not optimized) have been fabricated and characterized with a R_{DSoff}/R_{DSon} ratio evaluated at ca 1.5×10^3. This value appears to be significantly high to discriminate the off and the on state and highlights the potential of this new family of materials to construct embedded circuits.

ACKNOWLEDGMENTS

MC wishes to thank the Agence National de la Recherche (Project ANR *HOME-OLED n°ANR-11-BS07-020-01*) for a studentship. CP wishes to thank the UMR CNRS 6226-Institut des Sciences Chimiques de Rennes for an 'Inter UMR' grant. We thank the Region Bretagne and the Agence de l'Environnement et de la Maîtrise de l'Energie (ADEME) for a studentship (MR), the University of Rennes 1 for financial support (*Action Incitative* 2013), Sébastien Thiery (Rennes) for his help in organic synthesis and photophysical characterization, the

C.R.M.P.O. (Rennes) for mass analysis, the GENCI for allocation of computing time under project c2015085032 and the ISA (Lyon) for TGA analysis.

REFERENCES

1 C. Wang, H. Dong, W. Hu, Y. Liu, D. Zhu, *Chem. Rev.* 2012, **112**, 2208.
2 H. Usta, A. Facchetti, T. J. Marks, *Acc. Chem. Res.* 2011, **44**, 501.
3 Q. Meng, W. Hu, *Phys. Chem. Chem. Phys.* 2012, **14**, 14152.
4 K. Zhou, H. Dong, H.-L. Zhang, W. Hu, *Phys. Chem. Chem. Phys.* 2014, **16**, 22448.
5 Y. Xu, C. Liu, D. Khim, Y.-Y. Noh, *Phys. Chem. Chem. Phys.* 2015, **in press DOI 10.1039/c4cp02413c**.
6 M. J. Powell, *IEEE T. Electron. Dev.* 1989, **36**, 2753.
7 X. Gao, Y. Hu, *J. Mater. Chem. C* 2014, **2**, 3099.
8 D. Thirion, J. Rault-Berthelot, L. Vignau, C. Poriel, *Org. Lett.* 2011, **13**, 4418.
9 C. Poriel, J.-J. Liang, J. Rault-Berthelot, F. Barrière, N. Cocherel, A. M. Z. Slawin, D. Horhant, M. Virboul, G. Alcaraz, N. Audebrand, L. Vignau, N. Huby, G. Wantz, L. Hirsch, *Chem. Eur. J.* 2007, **13**, 10055.
10 N. Cocherel, C. Poriel, L. Vignau, J.-F. Bergamini, J. Rault-Berthelot, *Org. Lett.* 2010, **12**, 452.
11 C. Poriel, J. Rault-Berthelot, D. Thirion, *J. Org. Chem.* 2013, **73**, 886.
12 D. Thirion, C. Poriel, J. Rault-Berthelot, F. Barrière, O. Jeannin, *Chem. Eur. J.* 2010, **16**, 13646.
13 Y. Park, J.-H. Lee, D. H. Jung, S.-H. Liu, Y.-H. Lin, L.-Y. Chen, C.-C. Wu, J. Park, *J. Mater. Chem.* 2010, **20**, 5930.
14 J. Jacob, J. Zhang, A. C. Grimsdale, K. Müllen, M. Gaal, E. J. W. List, *Macromolecules* 2003, **36**, 8240.
15 C. Poriel, N. Cocherel, J. Rault-Berthelot, L. Vignau, O. Jeannin, *Chem. Eur. J.* 2011, **17**, 12631.
16 H. Usta, A. Facchetti, T. J. Marks, *J. Am. Chem. Soc.* 2008, **130**, 8580.
17 H. Usta, A. Facchetti, T. J. Marks, *Org. Lett.* 2008, **10**, 1385.
18 H. Usta, C. Risko, Z. Wang, H. Huang, M. K. Deliomeroglu, A. Zhukhovitskiy, A. Facchetti, T. J. Marks, *J. Am. Chem. Soc.* 2009, **131**, 5586.
19 Y.-I. Park, J. S. Lee, B. J. Kim, B. Kim, J. Lee, D. H. Kim, S.-Y. Oh, J. H. Cho, J.-W. Park, *Chem. Mater.* 2011, **23**, 4038.
20 T. Nakagawa, D. Kumaki, J.-I. Nishida, S. Tokito, Y. Yamashita, *Chem. Mater.* 2008, **20**, 2615.
21 J.-I. Nishida, S. Tsukaguchi, Y. Yamashita, *Chem. Eur. J.* 2012, **18**, 8964.
22 A. Shimizu, R. Kishi, M. Nakano, D. Shiomi, K. Sato, T. Takui, I. Hisaki, M. Miyata, Y. Tobe, *Angew. Chem. Int. Ed.* 2013, **52**, 6076.
23 D. T. Chase, B. D. Rose, S. P. Mc Clintock, L. N. Zakharov, M. M. Haley, *Angew. Chem. Int. Ed.* 2011, **50**, 1127.
24 A. Shimizu, Y. Tobe, *Angew. Chem. Int. Ed.* 2011, **50**, 6906.
25 A. G. Fix, P. E. Deal, C. L. Vonnegut, B. D. Rose, L. N. Zakharov, M. M. Haley, *Org. Lett.* 2013, **15**, 1362.
26 D. Thirion, M. Romain, J. Rault-Berthelot, C. Poriel, *J. Mater. Chem.* 2012, **22**, 7149.
27 D. Thirion, C. Poriel, R. Métivier, J. Rault-Berthelot, F. Barrière, O. Jeannin, *Chem. Eur. J.* 2011, **17**, 10272.
28 C. Poriel, J. Rault-Berthelot, D. Thirion, F. Barrière, L. Vignau, *Chem. Eur. J.* 2011, **17**, 14031.
29 C. Poriel, R. Métivier, J. Rault-Berthelot, D. Thirion, F. Barrière, O. Jeannin, *Chem. Commun.* 2011, **47**, 11703.

30 M. Romain, D. Tondelier, J.-C. Vanel, B. Geffroy, O. Jeannin, J. Rault-Berthelot, R. Métivier, C. Poriel, *Angew. Chem. Int. Ed.* 2013, **52**, 14147.
31 M. Romain, S. Thiery, A. Shirinskaya, C. Declairieux, D. Tondelier, B. Geffroy, O. Jeannin, J. Rault-Berthelot, R. Métivier, C. Poriel, *Angew. Chem. Int. Ed.* 2015, **54**, 1176.
32 C. B. Nielsen, E. Voroshazi, S. Holliday, K. Cnops, B. P. Rand, I. Mc Culloch *J. Mater. Chem. A* 2013, **1**, 73.
33 J.-I. Nishida, H. Deno, S. Ichimura, T. Nakagawa, Y. Yamashita, *J. Mater. Chem.* 2012, **22**, 4483.
34 E. Jacques, M. Romain, A. Yassin, S. Bebiche, M. Harnois, T. Mohammed-Brahim, J. Rault-Berthelot, C. Poriel, *J. Mater. Chem. C* 2014, **2**, 3292.
35 I. N. Levine, *Physical Chemistry*-, 5th Edition, Mc Graw-Hill, **2002**.
36 J. Rault-Berthelot, C. Poriel, F. Justaud, F. Barrière, *New J. Chem.* 2008, **32**, 1259.
37 N. Cocherel, C. Poriel, J. Rault-Berthelot, F. Barrière, N. Audebrand, A. M. Z. Slawin, L. Vignau, *Chem. Eur. J.* 2008, **14**, 11328.
38 M. Zhang, C. Yang, A. K. Mishra, W. Pisula, G. Zhou, B. Schmaltz, M. Baumgarten, K. Müllen, *Chem. Commun.* 2007, 1704.
39 L. Oldridge, M. Kastler, K. Müllen, *Chem. Commun.* 2006, 885.
40 M. Kosaki, Y. Yonezawa, K. Okada, *Org. Lett.* 2002, **4**, 4535.
41 M. Egginger, S. Bauer, R. Schwödiauer, H. Neugebauer, N. S. Sarifici, *Monatsh. Chem.* 2009, **140**, 735.
42 J. H. Park, Y. T. Lee, H.-S. lee, J.-Y. Lee, K. Lee, G.-B. Lee, J. Han, T. W. Kim, S. Im, *ACS Appl. Mater. Interfaces* 2013, **5**, 1625.
43 H. Sirringhaus, *Adv. Mater.* 2009, **21**, 3859.
44 j. Yuan, J. Zhang, J. Wang, D. Yan, W. Xu, *Thin Solid Films* 2004, **450**, 316.
45 W. A. Schoonveld, J. B. Oostinga, J. Vrijmoeth, T. M. Klapwijk, *Synth. Met.* 1999, **101**, 608.
46 X.-H. Zhang, B. Kippelen, *J. Appl. Phys.* 2008, **104**, 104504.
47 M. Mamada, H. Shima, Y. Yoneda, T. Shimano, N. Yamada, K. Kakita, T. Machida, Y. Tanaka, S. Aotsuka, D. Kumaki, S. Tokito, *Chem. Mater.* 2015, **27**, 141.